RMetS
Royal Meteorological Society

The influence of diabatic heating in the South Pacific Convergence Zone on Rossby wave propagation and the mean flow

Karin van der Wiel,[a,b]* Adrian J. Matthews,[a,b,c] Manoj M. Joshi[a,b,d] and David P. Stevens[a,c]

[a]*Centre for Ocean and Atmospheric Sciences, University of East Anglia, Norwich, UK*
[b]*School of Environmental Sciences, University of East Anglia, Norwich, UK*
[c]*School of Mathematics, University of East Anglia, Norwich, UK*
[d]*Climatic Research Unit, University of East Anglia, Norwich, UK*

*Correspondence to: K. van der Wiel, School of Environmental Sciences, University of East Anglia, Norwich Research Park, Norwich, NR4 7TJ, UK. E-mail: k.van-der-wiel@uea.ac.uk

The South Pacific Convergence Zone (SPCZ) is a northwest-southeast oriented precipitation band over the South Pacific Ocean. Latent heat release from condensation leads to substantial diabatic heating, which has potentially large impacts on local and global climate. The influence of this diabatic heating within the SPCZ is investigated using the Intermediate General Circulation Model (IGCM4).

Precipitation in the SPCZ has been shown to be triggered by transient Rossby waves that originate in the Australian subtropical jet and are refracted towards the equatorial eastern Pacific. A Rossby wave triggers a SPCZ 'convective event', with associated diabatic heat release and vortex stretching. Consequently, the Rossby wave is dissipated in the SPCZ region. These features are simulated well in a control integration of IGCM4.

In an experiment, convective heating is prescribed to its 'climatological' value in the SPCZ region during the Rossby wave 'events' and dynamic forcing from Rossby waves is decoupled from the usual thermodynamic response. In this experiment Rossby waves over the SPCZ region are not dissipated, confirming the vortex stretching mechanism from previous studies. Furthermore, the change in Rossby wave propagation has an impact on momentum transport. Overall, the effect of the Rossby wave-induced convection in the SPCZ is to decrease the strength of the Pacific subtropical jet and the equatorial eastern Pacific upper-tropospheric westerlies, by about 2–6 m s^{-1}.

Following these changes to the basic state, two potential feedbacks in the SPCZ and larger Pacific climate system are suggested: increased SPCZ convection due to the enhancement of negative zonal stretching deformation in the SPCZ region and decreased equatorward refraction of Rossby waves into the westerly duct leading to less SPCZ 'events'. As the convective events in the SPCZ have a significant impact on Pacific mean climate, it is crucial that the SPCZ is represented correctly in climate models.

Key Words: SPCZ; diabatic heating; tropical-extratropical interaction; Rossby waves

Received 20 April 2015; Revised 6 September 2015; Accepted 15 October 2015; Published online in Wiley Online Library 15 December 2015

1. Introduction

During austral summer, the South Pacific Convergence Zone (SPCZ) is a distinct feature in the distribution of precipitation over the southwestern Pacific Ocean (Figure 1(a)). It stretches diagonally, northwest-southeast, from New Guinea to about 30°S, 120°W in the central Pacific Ocean (Vincent, 1994). Its diagonal orientation is fundamentally different from the zonally oriented Intertropical Convergence Zone (ITCZ) in the northern hemisphere. The SPCZ provides vital precipitation to many Pacific island states. Past changes in its strength or position due to intraseasonal (e.g. the Madden-Julian Oscillation, MJO), interannual (e.g. El Niño-Southern Oscillation, ENSO) or interdecadal (e.g. the Interdecadal Pacific Oscillation, IPO) variability have had significant influences on the region (Griffiths *et al.*, 2003; Kumar *et al.*, 2006; Vincent *et al.*, 2011; Cai *et al.*, 2012; Haffke and Magnusdottir, 2013; Murphy *et al.*, 2014).

The large-scale SPCZ precipitation pattern was first observed when satellite images became available (Hubert, 1961; Streten, 1973). Since then, many studies have shown that tropical-extratropical interactions by means of transient Rossby waves are related to SPCZ precipitation (e.g. Trenberth, 1976; Kiladis and Weickmann, 1992, 1997; Matthews *et al.*, 1996; Widlansky *et al.*, 2011; Matthews, 2012; Van der Wiel *et al.*, 2015a). Atmospheric

© 2015 Royal Meteorological Society

processes on intraseasonal and interannual time scales (e.g. MJO, ENSO) set an atmospheric mean state on which synoptic Rossby waves propagate (Meehl *et al.*, 2001). Rossby wave propagation is limited to areas where the mean zonal wind field ($\overline{u}$) is westerly relative to the phase speed of the wave (c), i.e. $\overline{u} - c > 0$. At the boundary $\overline{u} - c = 0$ Rossby waves are evanescent; in areas of mean relative easterly winds ($\overline{u} - c < 0$) there will be no influence by Rossby waves from outside this region. Zonal and meridional asymmetries of the atmospheric mean state direct propagating Rossby waves, e.g. jet streams can act as a wave guide, and the upper-tropospheric westerly winds over the equatorial east Pacific and Atlantic (the 'westerly ducts') play an important role in steering waves exiting the jet (Hoskins and Ambrizzi, 1993; Ambrizzi *et al.*, 1995). Transient Rossby waves are a crucial part of the tropical momentum balance (Kiladis, 1998).

Besides tropical-extratropical interactions, other (local) processes have also been suggested to impact the SPCZ. The direct atmospheric impact of land-sea contrasts and orography is minimal (Kiladis *et al.*, 1989; Widlansky *et al.*, 2011; Van der Wiel *et al.*, 2015b). However, the blocking effect of the Andes mountain range enhances subsidence and cools Sea Surface Temperatures (SSTs) locally over the eastern Pacific. Both processes result in an enhancement of the east Pacific dry-zone, which influences the eastern margin of the SPCZ (Takahashi and Battisti, 2007a,2007b; Lintner and Neelin, 2008; Niznik and Lintner, 2013). Moisture transport and convergence in the lower troposphere are important factors in establishing the SPCZ diagonal orientation (Van der Wiel *et al.*, 2015b).

In Matthews (2012) and Van der Wiel *et al.* (2015a) observational-based data products are used to develop a framework to describe a mechanism that forces diagonal bands of convective precipitation in the SPCZ. Rossby waves from the Australian subtropical jet are refracted towards the westerly duct over the equatorial eastern Pacific. In this process, initial circular vorticity centres are elongated and develop a northwest-southeast, diagonal, orientation, caused by advection by the mean flow and Rossby refraction (Hoskins *et al.*, 1983; Van der Wiel *et al.*, 2015a). Ahead of cyclonic vorticity centres poleward flow enhances ascent in a band parallel to the diagonally oriented cyclone. In the tropical conditionally unstable atmosphere this triggers deep convection. Latent heat release in the convection enhances the ascending motions. The upper-tropospheric divergence associated with the convection and ascent is a source of anticyclonic vorticity through vortex stretching. The propagating cyclonic vorticity centres encounter this anticyclonic tendency; consequently the cyclones are weakened and dissipated in situ.

In this framework, Rossby waves ultimately dissipate themselves by means of a negative feedback involving convection and diabatic heating due to latent heat release from condensation. This is consistent with the observation of Trenberth (1976) that the SPCZ area acts as a 'graveyard region for fronts moving from the southwest'. This is associated with the deceleration of Rossby waves over the SPCZ area due to negative zonal stretching deformation in the basic state ($\partial U/\partial x < 0$), as discussed by Widlansky *et al.* (2011). Here, we will test the validity of the proposed framework in an Atmospheric General Circulation Model (AGCM) of intermediate complexity. Furthermore, we will investigate the influence of diabatic heating from convective events in the SPCZ on the regional mean flow. Tropical convection and associated heating is a substantial source of energy, the dynamical responses to this forcing has been the topic of many studies. Theoretically, the Gill-Matsuno model explains the generation and development of an equatorial Kelvin and Rossby wave response to localised tropical heating (e.g. as observed in the MJO, Matsuno, 1966; Gill, 1980). However, the dynamical response to tropical heating is not limited to the tropics (e.g. Qin and Robinson, 1993; Jin and Hoskins, 1995; Matthews *et al.*, 2004). The explicit influence of diabatic heating within the SPCZ has, to the authors knowledge, not been investigated before. Following the SPCZ mechanism in the framework of Matthews (2012) and Van der Wiel *et al.* (2015a), an AGCM experiment has been designed in which the thermodynamical response to dynamical Rossby wave forcing is removed in the SPCZ region. Potential changes to the Rossby wave and the south Pacific mean flow will be investigated. In section 2 the AGCM used in the experiments is described. The perturbation experiment is explained in more detail in section 3. The results are described in section 4 and finally the findings are summarised in section 5.

2. Model description

The Intermediate General Circulation Model version 4 (IGCM4, Joshi *et al.*, 2015) has been used in this study. It is an AGCM of intermediate complexity, i.e. within the hierarchy of climate models it has simpler parametrisation schemes than state-of-the-art AGCMs (e.g. the AGCMs in the Coupled Model Intercomparison Project phase 5, CMIP5). This makes the model well-suited for idealised experiments to increase process-level understanding.

IGCM4 is used here in its T42L20 configuration, i.e. 128 cells in longitude and 64 cells in latitute in the horizontal grid and 20 layers in the vertical. A monthly mean climatological seasonal cycle of SST, based on NOAA's Optimum Interpolation V2 dataset, is prescribed (Reynolds *et al.*, 2002, mean over 1982–2009). Land surface temperatures are computed self-consistently from surface fluxes (Forster *et al.*, 2000). IGCM4 runs the Morcrette radiation scheme (Zhong and Haigh, 1995) once for each model day. The parametrization for convective adjustment is based on the scheme of Betts (1986), it is slightly modified as described in Joshi *et al.* (2015). Cloud cover is computed to match observed profiles of convective clouds (Slingo, 1987); there is no aerosol forcing. A more detailed description of the physical parametrizations in IGCM4 is given in Joshi *et al.* (2015).

The November to April time mean precipitation for observations and in the IGCM4 control integration are in good agreement (Figure 1). Data from the CPC merged analysis precipitation (CMAP) project have been used here as observations (Xie and Arkin, 1997, mean over 1982–2009). Globally the quality of simulated precipitation in IGCM4 is within the range of CMIP5 atmosphere-only ('AMIP') experiments (Joshi *et al.*, 2015). For the current study it is more relevent that SPCZ location and orientation are simulated well in IGCM4, though the simulated precipitation rate within the SPCZ is slightly lower than observed (Figure 1).

3. Experimental design

3.1. Control integration

The aim of the current paper is to investigate the influence of diabatic heating from convective activity in the SPCZ on other aspects of the Pacific climate. With this in mind we have designed a perturbation experiment in which SPCZ convective events are removed. The experiment is based on the transient wave - convection framework (Matthews, 2012; Van der Wiel *et al.*, 2015a). Figure 2 shows a flow diagram that depicts the consecutive steps in the experiment, each described in more detail below.

First, an IGCM4 control integration was conducted. This integration was 17 years long, from which the first year was removed as spin-up. The remaining 16 years of data contained 15 full November to April seasons (step 1 in Figure 2). Within these seasons, 140 SPCZ 'convective events' were selected, based on Empirical Orthogonal Functions (EOFs). EOF spatial patterns of variability were computed from daily anomalies of Outgoing Longwave Radiation (OLR) in a box over the SPCZ region (180 to 120°W, 5–30°S, rectangle in Figure 3). In the tropics, OLR can be used as a proxy for precipitation; lower values are associated with colder temperatures, higher cloud tops and enhanced deep convection, higher values with warmer temperatures, lower cloud

© 2015 Royal Meteorological Society

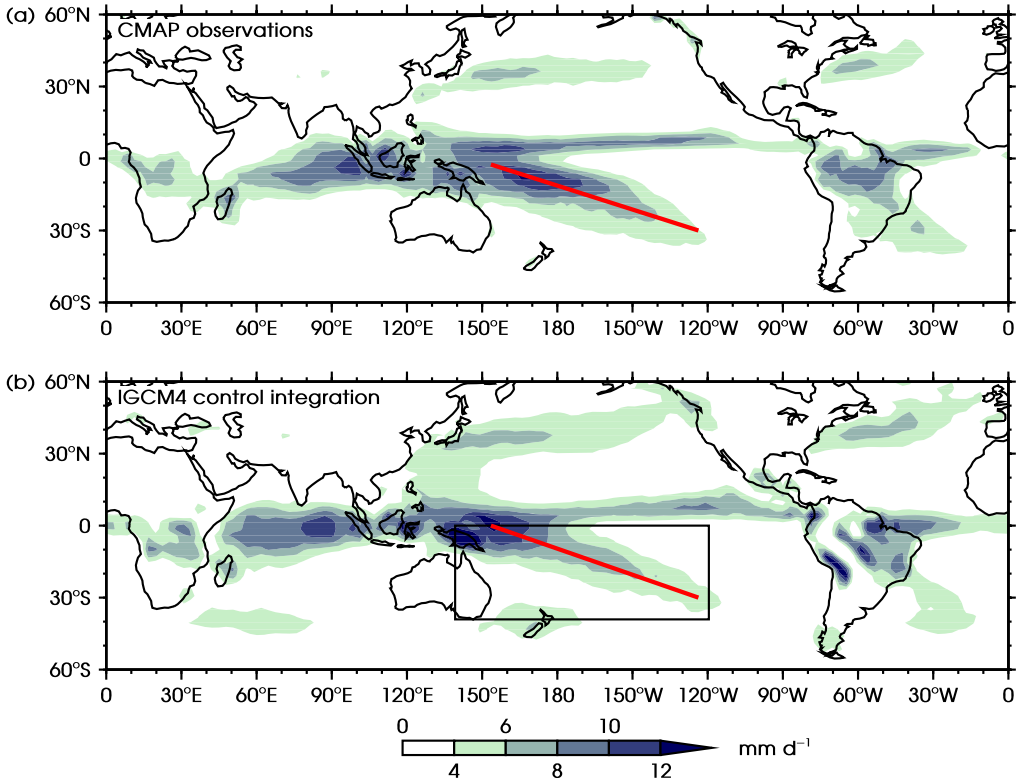

Figure 1. Time mean precipitation rate (November to April) in (a) CMAP and (b) the IGCM4 control integration (mm day^{-1}). The thick diagonal red lines show the position of the mean SPCZ precipitation axis, the rectangle in (b) shows the region for the perturbation experiment.

tops and reduced deep convection. The Principle Component (PC) time series associated with EOF 1 is then used for the selection of the convective events. If the value of the PC was above 1 standard deviation and was a local maximum relative to 5 days before and 5 days after that day, it was selected as a convective event (step 2 in Figure 2).

In the control integration, the computed temperature tendencies in the deep convection routine were saved at every timestep. These temperature tendency data were used to compute a three-dimensional monthly varying climatology (step 3 in Figure 2), to be used in the perturbation experiment.

3.2. *Perturbation experiment*

The perturbation experiment aims to prevent dynamical forcing from Rossby waves from generating the observed anomalous diabatic heating response in the SPCZ region (Matthews, 2012; Van der Wiel *et al.*, 2015a). The experiment is based on 140 restart integrations started 4 days before each of the 140 selected convective events in step 2. At this time (event −4 days) the dynamical transient Rossby wave forcing is present, but the convective response in the SPCZ region has not commenced. From this atmospheric state a modified IGCM4 was integrated for 14 days (i.e. up to 10 days after the event). In the modified model all grid cells overlying ocean in the SPCZ region (140°E to 120° W, 0–40°S, rectangle in Figure 1(b)) have the deep convective temperature tendency prescribed from the precalculated climatological tendency in step 3 rather than computed self-consistently within the model code; i.e. instead of allowing the deep convection scheme to compute temperature tendencies, the climatological values were used. Moisture tendencies and precipitation were computed as normal to avoid an unrealistic build up or removal of moisture. Outside the SPCZ region the model code was integrated as normal. The perturbation experiment is the composite mean of all restart integrations (step 4 in Figure 2).

In the next section results from the different steps are discussed separately. Steps 1 and 2 will be discussed in section 4.1, step 3 in section 4.2 and finally step 4 in sections 4.3 and 4.4.

4. Experimental results

4.1. *Transient wave - convection feedback in control integration*

The first mode of variability from EOF analysis (7.8% of total variance) shows enhanced convection (negative OLR anomalies) shifted to the southwest, however it remains parallel to the SPCZ mean precipitation axis (Figure 3(a)). To the northeast a parallel band of reduced convection is found. The second mode of variability (7.3%, not shown, well-separated from EOF1 and further EOFs, North *et al.*, 1982) shows enhanced convection over the mean precipitation axis and reduced convection to the southwest. These 'southwestward shifted' and 'enhanced' convection patterns are comparable to patterns found in observational data (e.g. Vincent *et al.*, 2011; Matthews, 2012; Salinger *et al.*, 2014; Van der Wiel *et al.*, 2015a).

Following the criteria presented in section 3, 140 events of the southwestward shifted mode have been selected from the EOF 1 PC time series (Figure 3(b)). Composite means were computed by taking the mean of a field over all event days. Anomalies of 200 hPa vorticity and precipitation for these convective events are shown in Figure 4. Four days before the event a Rossby wave train is present south of Australia. As was found in observational-based data, over the following days, the wave is refracted along a curved path towards the equatorial east Pacific. During this process the combined effect of advection by the mean wind, shear on the equatorward edge of the jetstream and Rossby wave refraction changes the shape of the vorticity centres (Van der Wiel *et al.*, 2015a); the centres develop a northwest-southeast diagonal orientation, parallel to the SPCZ mean precipitation axis (Figure 4(b)). This process is further supported by the meridional stretching deformation of the basic state (Widlansky, 2010).

Two days before the convective event the Rossby wave initiates enhanced precipitation. Ahead of a cyclonic vorticity anomaly, poleward wind ascends and in the tropical conditionally unstable atmosphere this triggers deep convection. The vorticity centre propagates northeastward with the Rossby wave, the associated precipitation signal remains ahead of the cyclone at all times. At the day of the convective event, by design

© 2015 Royal Meteorological Society

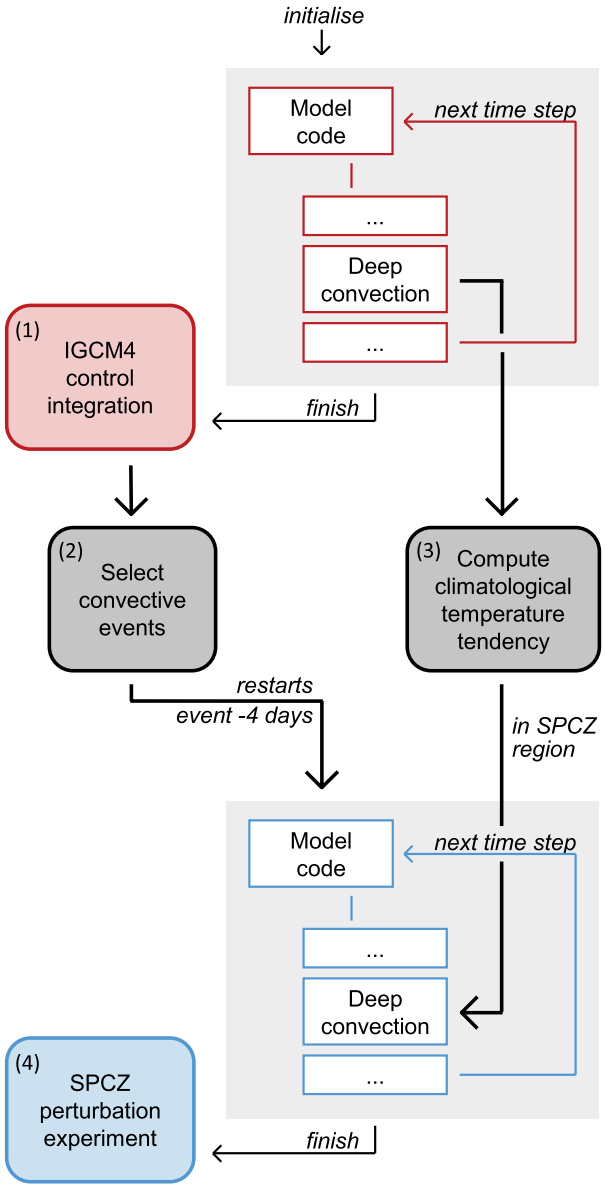

Figure 2. Flow diagram of experimental setup; detailed explanations of each step numbered (1) through (4) are provided in the main text (section 3).

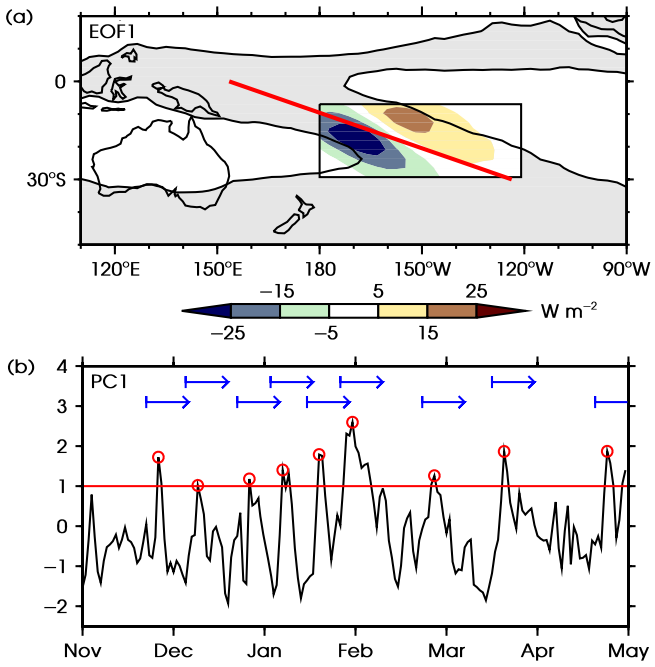

Figure 3. (a) EOF pattern 1 in shaded colours (W m^{-2}) in the rectangular box, overlaid on the time mean OLR field (November to April, grey shading is <250 W m^{-2}). The thick diagonal red line shows the position of the SPCZ mean precipitation axis. (b) Sample time series of the PC associated with EOF 1 during November-April of model integration year 10. The red line and circles show the selection of SPCZ convective events, blue arrows show the duration of the associated restart integrations.

of the composite method, the precipitation anomaly reaches a maximum (~10 mm day^{-1}) and the pattern resembles the southwestward shifted pattern of EOF 1; there is a diagonal band of enhanced precipitation to the southwest of the SPCZ mean precipitation axis and reduced precipitation to the northeast. Two days after the convective event the precipitation anomalies have mostly disappeared (Figure 4(d)).

The diabatic heat release from the precipitation anomalies is substantial and enhances ascending motions and upper-tropospheric divergence. Through vortex stretching this acts as a negative feedback, $\partial\zeta/\partial t = -fD$, where ζ is relative vorticity, t is time, f is the Coriolis parameter and D is divergence, and results in an anticyclonic tendency: the propagating cyclone in the Rossby wave is dissipated. Consequently, Rossby wave propagation is disturbed downstream of the SPCZ region. The effect is clear in the evolution of the vorticity centres in the Rossby wave in Figure 4, at the moment precipitation anomalies are triggered propagation of the upstream cyclonic vorticity centre slows down and weakens. The Rossby wave favours a more southern propagation path, back towards the wave guide in the jet, where both precipitation anomalies and the negative feedback effect are weaker. Two days after the convective event the wave is mostly dissipated.

The sequence of events forcing diagonally oriented bands of precipitation in the IGCM4 control integration is similar to the sequence found using similar methods and observational-based data products (Matthews, 2012; Van der Wiel *et al.*, 2015a). The realistic representation of this process makes IGCM4 a suitable AGCM for the perturbation experiment.

4.2. *Diabatic heating from deep convection*

The simulated November to April time mean mid-tropospheric climatological heating due to deep convection is shown in Figure 5(a). Higher values of diabatic heating are found at locations with frequent convective precipitation, lower values in areas of less precipitation (Figures 1(b), 5(a)). The SPCZ, ITCZ, South Atlantic Convergence Zone (SACZ) and South Indian Convergence Zone can all be identified as areas of enhanced diabatic heating from deep convection. The south Pacific dry zone has very weak diabatic heating from deep convection.

Figure 5(b) and (c) show vertical sections of the same quantity. The black areas on the cross-section show the grid cells where the IGCM4 deep convection scheme has not once been initiated in the 15 seasons included in the control integration (effectively the stratosphere). For these cells a climatological heating of 0 K $timestep^{-1}$ is assumed in the experimental integration. Along 155°E (Figure 5(b)) the region of most intense heating lies over the equator, where the SPCZ and ITCZ merge. In this region, there is a slight negative temperature tendency at the surface due to evaporative cooling, in the mid-troposphere there is substantial diabatic heating and near the model top (σ = 0.05) there is a negative temperature tendency due to radiative cooling. Further east at 149°W (Figure 5(c)) the heating profiles related to the SPCZ and ITCZ are weaker and separated and found at about 20°S and 8°N respectively.

These climatological temperature tendency data are used in the perturbation experiment. Instantaneous, self-consistent temperature tendencies are used in the control integration (left column of Figure 6). This heating pattern is more irregular than in the climatology, changes fast in time and has larger extremes. Following the earlier discussion, it can be seen that ahead of upper-tropospheric cyclonic vorticity anomalies convective heating is strongest. As the cyclone propagates northeastward this region

© 2015 Royal Meteorological Society

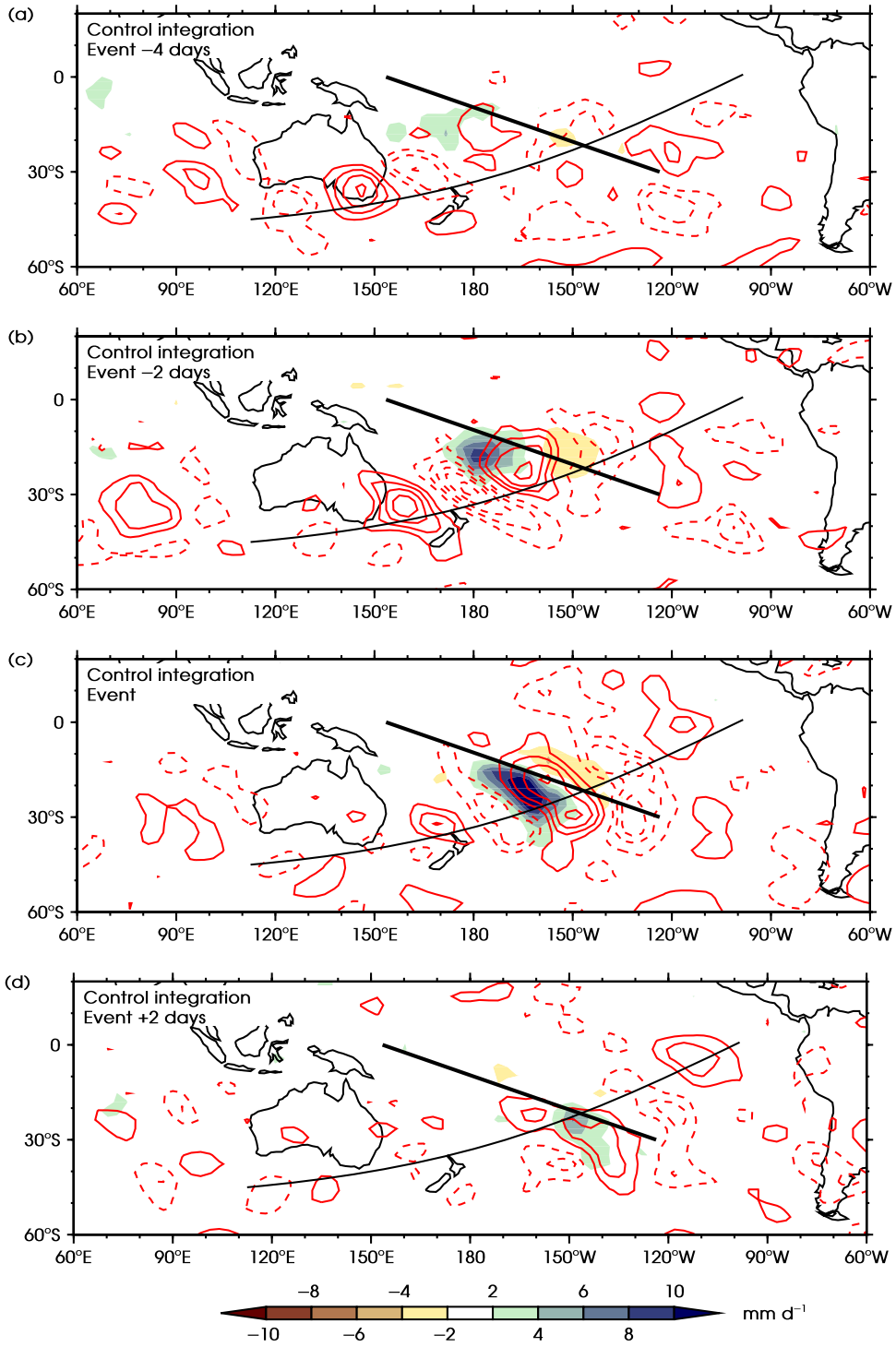

Figure 4. Composite mean anomalies over the 140 shifted SPCZ events of precipitation rate in shaded colours (mm day^{-1}), and 200 hPa vorticity in red contours (4×10^{-6} s^{-1} contour interval, zero contour omitted, negative contours dashed) for the IGCM4 control integration. The thick diagonal line indicates the position of the SPCZ mean precipitation axis, the curved line an approximate wave propagation path. Time lags shown: (a) event −4 days, (b) event −2 days, (c) event, and (d) event +2 days.

of enhanced heating also moves northeastward, similar to the progression of precipitation anomalies (Figure 4). Ahead of anticyclonic vorticity anomalies convective heating is weaker. In the perturbation experiment, as discussed in section 3, in the SPCZ region this instantaneous, self-consistent temperature tendency is replaced by the relevant climatological value from the seasonal cycle appropriate for each of the 140 restart integrations. The composite mean temperature tendencies as used in the experimental model integration are shown in the right column of Figure 6. Outside the rectangular SPCZ region there has been no change from the control integration (small differences due to separate integrations in control and experiment), inside the rectangular region instantaneous values have been replaced by climatological values (compare horizontal rows in Figure 6).

4.3. *Impact of diabatic heating on Rossby wave propagation*

As described in section 3, the restart integrations are initiated from the control integration at 4 days before the 140 selected convective events. At this moment a Rossby wave train is present south of Australia (Figure 7(a)). Two days into the perturbation experiment, the Rossby wave has propagated northeastward into the SPCZ region (Figure 7(b)). Ahead of the cyclonic anomaly is an anomalous poleward flow that leads to ascent along the sloping mean isentropes. There is a small anomalous precipitation signal associated with this ascent (∼2 mm day^{-1}). However, the associated anomalous diabatic heat release is removed in the experiment so no additional ascending motions are forced. This results in a much weaker precipitation rate in the

© 2015 Royal Meteorological Society

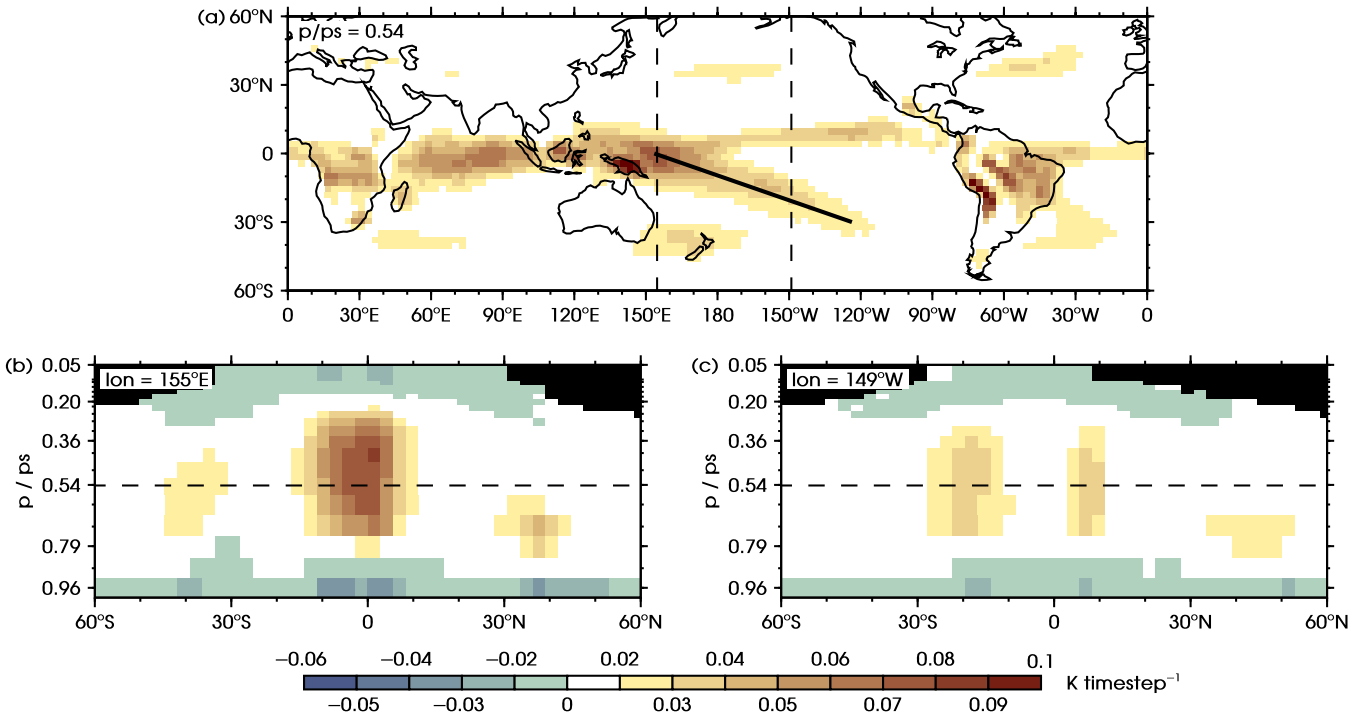

Figure 5. Time mean temperature tendency due to deep convection (November to April) in IGCM4 at (a) $p/ps = 0.54$, and vertical sections at (b) 155°E and (c) 149°W in shaded colours (K timestep^{-1}). Vertical levels are pressure (p) / surface pressure (ps) or sigma coordinates. Dashed lines in (a) show the locations of the vertical sections in (b,c), dashed lines in (b,c) show the level of the map in (a). The thick diagonal line in (a) shows the position of the mean SPCZ precipitation axis. Black areas signify areas where data is not available.

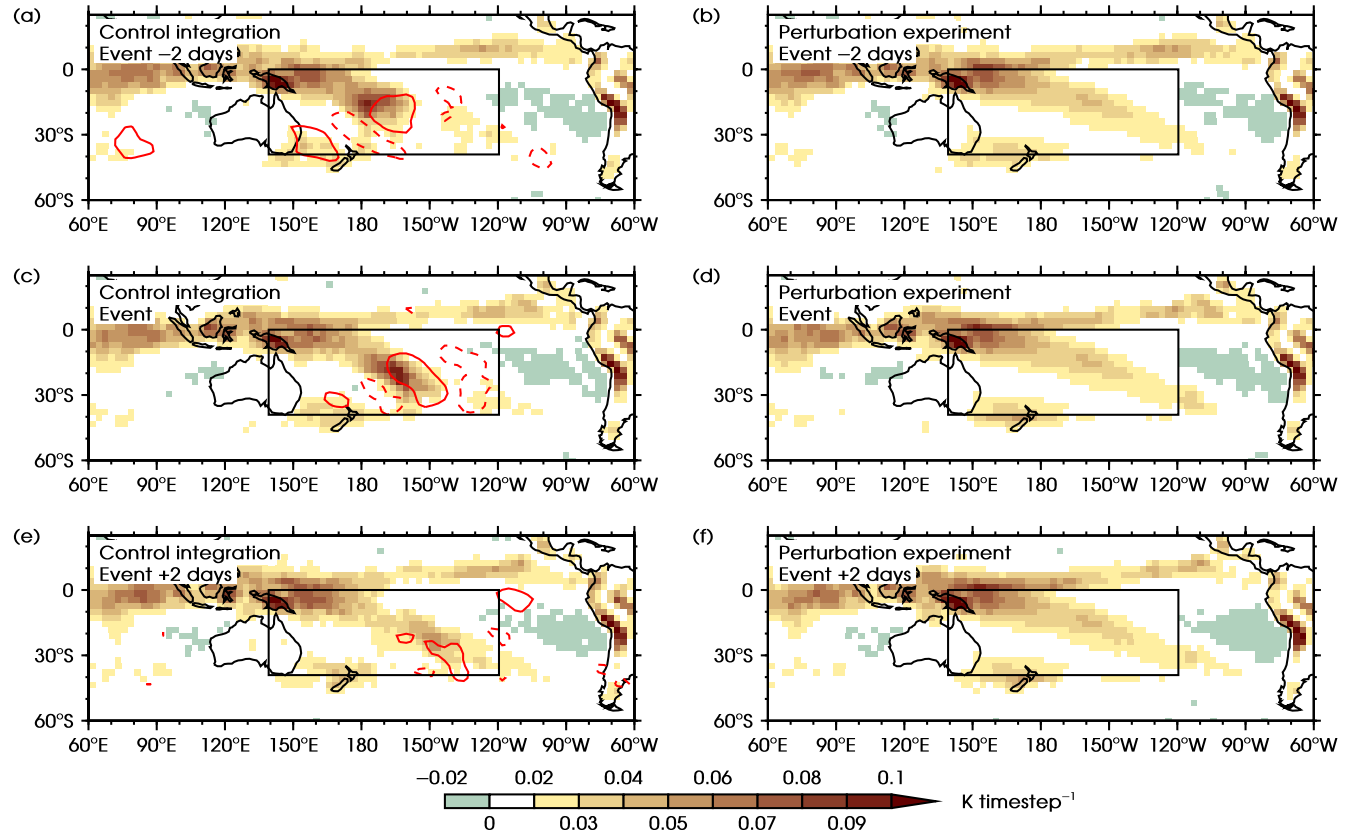

Figure 6. Composite mean temperature tendency due do deep convection at $p/ps = 0.54$ in shaded colours (K timestep^{-1}). (a,c,e) show the instantaneous, self-consistent model computed tendency in the control integration. In the perturbation experiment this is replaced by the climatological tendency within the experiment region (black rectangle) as shown in (b,d,f). Red contours in (a,c,e) show 200 hPa vorticity anomalies in the control integration (as in Figure 4, the 8×10^{-6} s^{-1} contour as a solid line, the -8×10^{-6} s^{-1} contour as a dashed line).

perturbation experiment than in the control integration at this point (~8 mm day^{-1}, Figure 4(b)).

In the following days this process continues. Vorticity centres in the wave propagate northeastward. Ahead of the cyclonic vorticity anomaly and along the SPCZ mean precipitation axis there is some anomalous precipitation. However, the precipitation rates are constant around ~2 mm day^{-1}; there is no distinct peak in precipitation rates at the convective event as was found in the control integration.

In the sequence of events that ultimately triggers diagonal bands of convective precipitation over the SPCZ region in the control integration, the negative feedback from vortex stretching

© 2015 Royal Meteorological Society

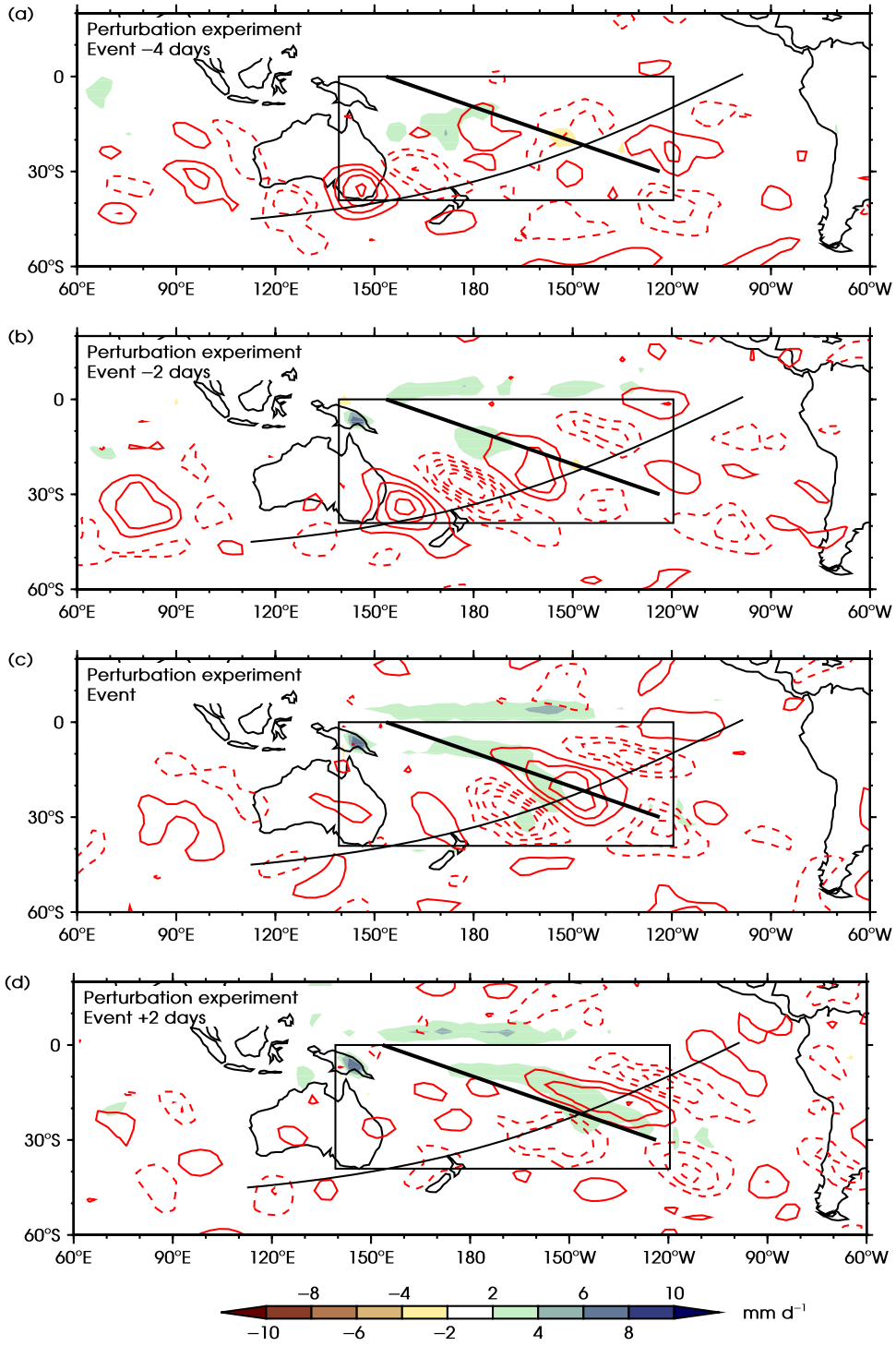

Figure 7. As Figure 4, but for the perturbation experiment. Note (a) is the same as Figure 4(a), the starting point of the pertubation experiment. The rectangle indicates the region for the perturbation experiment.

starts influencing Rossby wave propagation 2 days before the convective event. When the convective heating response is taken out of the sequence, diabatic heating, ascending motions and upper-tropospheric divergence are all significantly weaker than in the control integration. The maximum composite-mean upper-tropospheric divergence in the perturbation experiment is 4×10^{-6} s^{-1}, only 30% of the divergence in the control integration (13×10^{-6} s^{-1}). The negative feedback, $\partial\zeta/\partial t = -fD$, is therefore much weaker and has a smaller effect on the transient Rossby wave.

The northeastward propagation of the Rossby wave is undisturbed in the perturbation experiment. The vorticity centres are reformed due to shear and Rossby refraction as in the control integration, though the effects are more obvious in the experiment. Vorticity centres become elongated and rotate from a diagonal orientation (northwest-southeast) to a zonal orientation at the equator (Figure 7(c)). The southward tendency of the wave pattern in the control integration is not found in the experiment, instead Rossby wave propagation continues across the equator.

The propagation speed of the Rossby wave can be estimated from a Hovmöller diagram (Figure 8). The vorticity centres move eastward steadily at the phase speed; wave energy moves through the region at the faster group speed. In the perturbation experiment the phase speed is about 580 km day^{-1} $\approx$ 6.7 m s^{-1}, the group speed approximately 2000 km day^{-1} $\approx$ 23 m s^{-1} (grey dotted lines in Figure 8). These values are comparable in the control integration, however wave propagation downstream of the SPCZ mean precipitation axis is disturbed. The cyclone at 180° weakens when precipitation is triggered 2 days before the convective event, in the perturbation experiment the cyclone is present for longer and propagates further eastward. The same effect appears for the anticyclone at 160°W. In both model

© 2015 Royal Meteorological Society

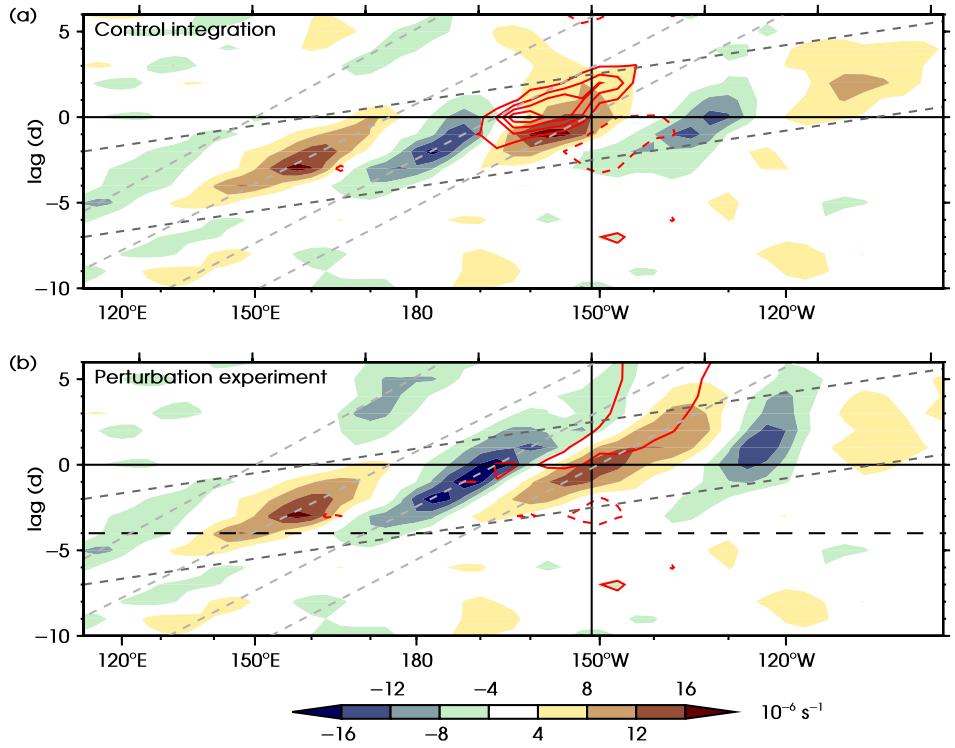

Figure 8. Hovmöller diagram of lagged composite anomalies along the curved propagation path in the (a) control integration (Figure 4) and (b) perturbation experiment (Figure 7). The 200 hPa vorticity is shown in shaded colours (10^{-6} s^{-1}) and precipitation in red contours (2 mm day^{-1} contour interval, zero contour omitted, negative contours dashed). The vertical solid line denotes the position of the mean SPCZ axis, the horizontal dashed line in (b) is the beginning of the restart integrations at event −4 days. Light grey dotted lines show the approximate phase speed, dark grey dotted lines the approximate group speed. Horizontal axes are irregular longitude (bottom) or regular distance (top, 2000 km intervals) along the path.

integrations propagation slows down close to the equator at about 130°W. Not visible in the Hovmöller diagram is the different shape of the Rossby waves after the convective events in the control integration and perturbation experiment (Figures 4(d) and 7(d)).

As precipitation rates decrease significantly in the perturbation experiment, there is a slight build up of moisture in the experimental region of up to 2 g kg^{-1} in specific humidity at 850 hPa. This moisture is advected by horizontal winds out of the experimental region. This results in enhanced precipitation over New Guinea and in a zonal line just north of the experimental region (Figure 7(c,d)), as the model computes convective temperature tendencies self-consistently there. The increased moisture content does increase modelled low level clouds and through a radiative feedback lowers surface temperatures in the SPCZ region slightly. The impact of this side effect on Rossby wave propagation in the experimental region is small.

4.4. *Impact of diabatic heating on the mean flow*

Six days after the convective event the Rossby wave has disappeared in both the control integration and in the perturbation experiment. In the control integration the upper-troposphere has returned to its 'normal' state (Figure 9(a)); anomalies of zonal wind speed are very small (less than 2 m s^{-1}). There is no coherent pattern to these anomalies over most of the Pacific Ocean, though there is a hint of a wave train over South America, from the southeast Pacific towards the equatorial Atlantic. A similar wave train has been linked to enhanced SACZ activity (e.g. Liebmann *et al.*, 1999; Robertson and Mechoso, 2000; Van der Wiel *et al.*, 2015a). By means of influence functions, Grimm and Silva Dias (1995) found a link between convection in the SPCZ and in the SACZ. However, no significant lagged correlations were found between convective events in the SPCZ and subsequent convective events in the SACZ in the IGCM4 control integration.

The post-convective event upper-tropospheric zonal wind anomalies in the perturbation experiment are much larger (Figure 9(b)). Along the Rossby wave propagation path and over the equatorial east Pacific there are strong positive (westerly) anomalies. To the north and south of the propagation path there are negative (easterly) anomalies. The anomaly pattern is approximately southwest-northeast, perpendicular to the prescribed heating pattern, which suggests it is not a direct effect in response to the prescribed heating but rather has a different, dynamical origin.

In the control integration and in the actual climate system, there are two processes that feedback from SPCZ activity onto the basic state wind. In general, tropical heating results in an off-equatorial anticyclone that accelerates the subtropical jets, through a Gill-like response (Gill, 1980). Additionally, the diagonal, northwest-southeast, orientation of the vorticity centres in the waves leads to a mean poleward transport of westerly momentum in these waves, as anomalies of the zonal and meridional wind are anticorrelated in the wave ($\overline{u'v'} < 0$, see also Kiladis, 1998). These two processes determine, in part, the strength of the modelled climatological subtropical jet at 30°S. The Gill-response and momentum transport by Rossby waves in the control run result in this climatological jet. The weak anomalies after the SPCZ events (Figure 9(a)) are just due to sampling variability.

In the perturbation experiment both processes are modified. Diabatic heating in the SPCZ region is limited, therefore the Gill anticyclone would be weaker and its acceleration of the subtropical jet would be decreased. However, this is not observed in the experiment (Figure 9(b)); the effect is off-set by the strengthened Rossby wave signal. Rossby wave propagation towards the SPCZ region and the westerly duct is enhanced, leading to increased poleward transport of westerly momentum and positive anomalies of zonal wind in the subtropical jet. Rossby wave propagation from the SPCZ region back towards the subtropical jet is less favoured in this state, resulting in weaker poleward momentum transport and negative zonal wind anomalies at 40°S, 120°W.

In the perturbation experiment the anomalous diabatic heating from SPCZ convection triggered by equatorward propagating Rossby waves has been switched *off*. Therefore, the climatological effect of this SPCZ convection on the basic state (contours in Figure 9(c)) will be the *opposite* of the effect in the perturbation experiment (Figure 9(b)). Dashed contours in

© 2015 Royal Meteorological Society

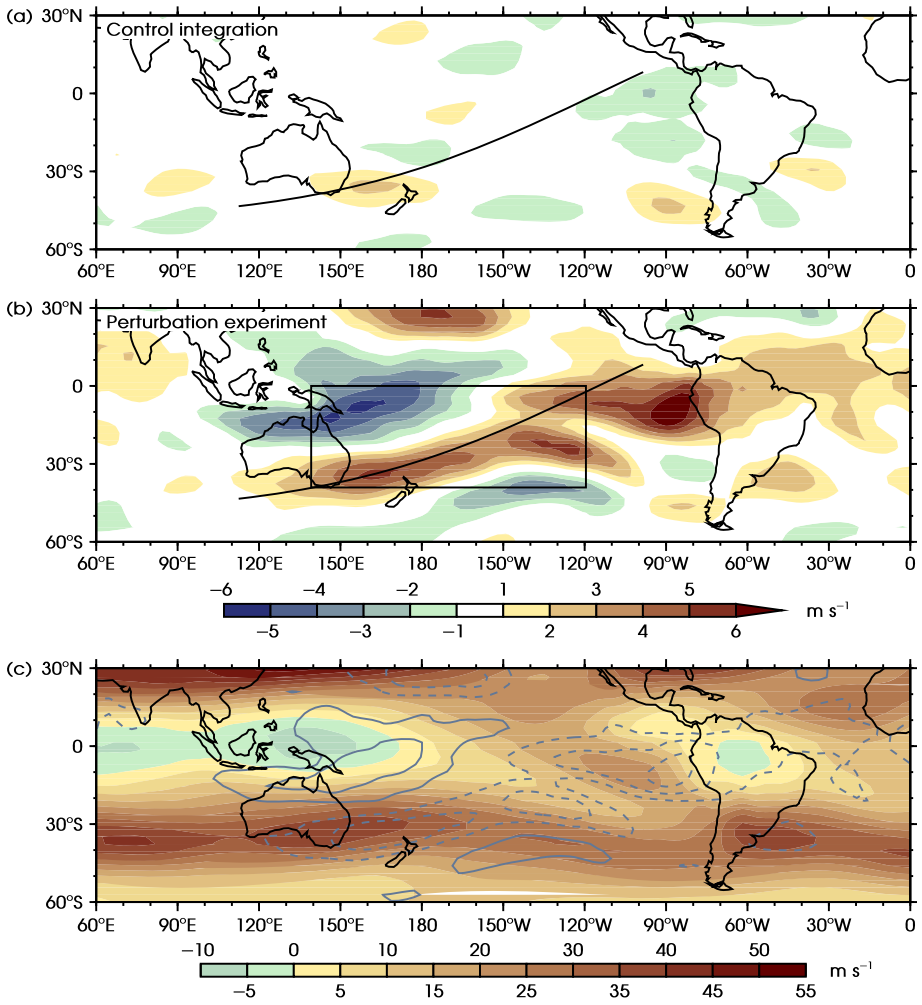

Figure 9. Mean 200 hPa zonal wind anomaly (m s^{-1}) over composite days event +6 days to event +10 days for the (a) control integration, and (b) the perturbation experiment. The curved line an approximate wave propagation path, the rectangle in (b) indicates the region for the perturbation experiment. (c) Time mean 200 hPa zonal wind (November to April) in the control integration in shaded colours (m s^{-1}) and SPCZ convective event wind anomaly (b) overlaid in grey contours, note the sign has been changed from (b) (2 m s^{-1} contour interval, zero contour omitted, negative contours dashed).

Figure 9(c) show areas where the climatological westerly winds are decreased in strength or where climatological easterly winds are increased in strength; solid contours show areas of increased westerly/decreased easterly winds. Therefore, convective events in the SPCZ act to decrease the strength of the subtropical jet and the westerly winds along the wave propagation path. This results in an enhancement of the region of negative stretching deformation near the SPCZ. Following the mechanism discussed in Widlansky *et al.* (2011), this would increase the accumulation of wave energy there and increase convection along the SPCZ. The described feedback would be positive: convective events in the SPCZ increase the likelihood of further convective events.

Furthermore, the strength of the westerly duct over the equatorial eastern Pacific is decreased. The westerly duct is partially responsible for the initial equatorward propagation of the Rossby waves. In the IGCM4 control integration the zonal wind speed in the westerly duct is ∼20 m s^{-1} (colours in Figure 9(c)), a change of ∼ −4 m s^{-1} due to SPCZ convection is an important factor in determining its strength. This feedback would be negative: convective events in the SPCZ decrease the likelihood of wave refraction towards the SPCZ and the westerly duct, decreasing the chance of a next convective event.

5. Discussion

The influence of convective events in the SPCZ on local Rossby wave propagation and the Pacific mean flow has been tested by means of an AGCM experiment. In observational data and in the control integration, Rossby waves trigger deep convection and precipitation in the SPCZ. In a perturbation experiment the dynamical Rossby wave forcing is decoupled from a potential thermodynamical response: instantaneous diabatic heating during SPCZ convective events is removed and replaced by a climatological value. Experimental results show continued Rossby wave propagation from the subtropical jet towards the eastern equatorial Pacific and across the equator. In the control integration and in observations these Rossby waves are dissipated in the SPCZ region due to diabatic heat release in the convection and a negative feedback due to vortex stretching. The continued Rossby propagation in the experiment provides additional evidence for the feedback mechanism in the transient wave-convection framework proposed by Matthews (2012) and Van der Wiel *et al.* (2015a).

Besides influencing transient Rossby waves locally, the experiment shows convective events in the SPCZ region have a significant impact on the south Pacific upper-tropospheric zonal wind climate. As discussed, in the control integration and in observations, convective events in the SPCZ hinder Rossby wave propagation in the region. Consequently the poleward transport of westerly momentum is decreased, as transient Rossby waves are an important factor in the tropical momentum balance (Kiladis, 1998). Convective events in the SPCZ act to weaken both the subtropical jet and the equatorial westerly duct. The first of these effects enhances the region of negative zonal stretching deformation potentially resulting in enhanced convection along the SPCZ (Widlansky *et al.*, 2011). The second reduces the equatorward refraction of Rossby waves that trigger SPCZ convective events (Van der Wiel *et al.*, 2015a). To determine the strength of these feedbacks requires further modelling experiments.

© 2015 Royal Meteorological Society

These results can be interpreted within the general framework of Meehl *et al.* (2001), where atmospheric processes on longer time scales and larger spatial scales set a mean atmospheric state on which synoptic waves propagate (the Rossby waves in the SPCZ in this example). In the general framework, processes on synoptic scales then influence atmospheric processes on synoptic time scales, but also on longer time and larger spatial scales. Here, this corresponds to the effect convective activity has on the atmospheric basic state through changed momentum transport.

SST biases in coupled models in the Coupled Model Intercomparison Project phase 5 (CMIP5) force a too zonal tropical part of the SPCZ, which then gives a more discontinuous simulated SPCZ than is observed (Brown *et al.*, 2011, 2013; Niznik *et al.*, 2015). Such biases influence future rainfall projections of the SPCZ (Widlansky *et al.*, 2013). Based on the results presented here, biases in the represented SPCZ lead to further biases in the representation of convective heating, Rossby wave propagation, momentum transport and the mean upper-tropospheric wind climate. Projections of changes in atmospheric processes in a future warmer climate are often based on these CMIP5 models, it is therefore of importance to improve the representation of the SPCZ in such models.

Acknowledgements

The CMAP data were provided by the NOAA/OAR/ESRL PSD, Boulder, Colorado, USA, from their web site at http://www.cdc.noaa.gov/. The research presented in this article was carried out on the High Performance Computing Cluster supported by the Research Computing Service at the University of East Anglia. The authors would like to thank George Kiladis and three anonymous reviewers for comments that helped to improve the manuscript.

References

Ambrizzi T, Hoskins BJ, Hsu H-H. 1995. Rossby wave propagation and teleconnection patterns in the austral winter. *J. Atmos. Sci.* **52**: 3661–3672.

Betts AK. 1986. A new convective adjustment scheme. Part I: Observational and theoretical basis. *Q. J. R. Meteorol. Soc.* **112**: 677–691.

Brown JR, Power SB, Delage FP, Colman RA, Moise AF, Murphy BF. 2011. Evaluation of the South Pacific Convergence Zone in IPCC AR4 climate model simulations of the twentieth century. *J. Clim.* **24**: 1565–1582.

Brown JR, Moise AF, Colman RA. 2013. The South Pacific Convergence Zone in CMIP5 simulations of historical and future climate. *Clim. Dyn.* **41**: 2179–2197.

Cai W, Lengaigne M, Borlace S, Collins M, Cowan T, McPhaden MJ, Timmermann A, Power S, Brown J, Menkes C, Ngari A, Vincent EM, Widlansky MJ. 2012. More extreme swings of the South Pacific Convergence Zone due to greenhouse warming. *Nature* **488**: 365–370.

Forster PM de F, Blackburn M, Glover R, Shine KP. 2000. An examination of climate sensitivity for idealised climate change experiments in an intermediate general circulation model. *Clim. Dyn.* **16**: 833–849.

Gill AE. 1980. Some simple solutions for heat-induced tropical circulation. *Q. J. R. Meteorol. Soc.* **106**: 447–462.

Griffiths GM, Salinger MH, Leleu I. 2003. Trends in extreme daily rainfall across the South Pacific and relationship to the South Pacific Convergence Zone. *Int. J. Climatol.* **23**: 847–869.

Grimm AM, Silva Dias PL. 1995. Analysis of tropical-extratropical interactions with influence functinos of a barotropic model. *J. Atmos. Sci.* **52**: 3538–3555.

Haffke C, Magnusdottir G. 2013. The South Pacific Convergence Zone in three decades of satellite images. *J. Geophys. Res.* **118**: 1–11, doi: 10.1002/jgrd.50838.

Hoskins BJ, Ambrizzi T. 1993. Rossby wave propagation on a realistic longitudinally varying flow. *J. Atmos. Sci.* **50**: 797–812.

Hoskins BJ, James IN, White GH. 1983. The shape, propagation and mean-flow interaction of large-scale weather systems. *J. Atmos. Sci.* **40**: 1595–1612.

Hubert LF. 1961. A subtropical convergence line of the South Pacific: A case study using meteorological satellite data. *J. Geophys. Res.* **66**: 1661–1671, doi: 10.1029/JZ066i003p00797.

Jin F, Hoskins BJ. 1995. The direct response to tropical heating in a baroclinic atmosphere. *J. Atmos. Sci.* **52**: 307–319.

Joshi MM, Stringer M, Van der Wiel K, O'Callaghan A, Fueglistaler S. 2015. IGCM4: A fast, parallel and flexible intermediate climate model. *Geosci. Model Dev.* **8**: 1157–1167.

Kiladis GN. 1998. Observations of Rossby waves linked to convection over the eastern tropical Pacific. *J. Atmos. Sci.* **55**: 321–339.

Kiladis GN, Weickmann KM. 1992. Extratropical forcing of tropical Pacific convection during northern winter. *Mon. Weather Rev.* **120**: 1924–1938.

Kiladis GN, Weickmann KM. 1997. Horizontal structure and seasonality of large-scale circulations associated with submonthly tropical convection. *Mon. Weather Rev.* **125**: 1997–2013.

Kiladis GN, von Storch H, van Loon H. 1989. Origin of the South Pacific Convergence Zone. *J. Clim.* **2**: 1185–1195.

Kumar VV, Deo RC, Ramachandran V. 2006. Total rain accumulation and rain-rate analysis for small tropical Pacific islands: A case study of Suva, Fiji. *Atmos. Sci. Lett.* **7**: 53–58.

Liebmann B, Kiladis GN, Marengo JA, Ambrizzi T, Glick JD. 1999. Submonthly convective variability over South America and the South Atlantic convergence zone. *J. Clim.* **12**: 1877–1891, doi: 10.1029/2008GL034298.

Lintner BR, Neelin JD. 2008. Eastern margin variability of the South Pacific Convergence Zone. *Geophys. Res. Lett.* **35**: L16701.

Matsuno T. 1966. Quasi-geostrophic motions in the equatorial area. *J. Meteorol. Soc. Jpn.* **44**: 25–42.

Matthews AJ. 2012. A multiscale framework for the origin and variability of the South Pacific Convergence Zone. *Q. J. R. Meteorol. Soc.* **138**: 1165–1178.

Matthews AJ, Hoskins BJ, Slingo JM, Blackburn M. 1996. Development of convection along the SPCZ within a Madden-Julian oscillation. *Q. J. R. Meteorol. Soc.* **122**: 669–688.

Matthews AJ, Hoskins BJ, Masutani M. 2004. The global response to tropical heating in the Madden-Julian oscillation during northern winter. *Q. J. R. Meteorol. Soc.* **130**: 1991–2011.

Meehl GA, Lukas R, Kiladis GN, Weickmann KM, Matthews AJ, Wheeler M. 2001. A conceptual framework for time and space scale interactions in the climate system. *Clim. Dyn.* **17**: 753–775.

Murphy BF, Power SB, McGree S. 2014. The varied impacts of El Niño-Southern Oscillation on Pacific island climates. *J. Clim.* **27**: 4015–4036.

Niznik MJ, Lintner BR. 2013. Circulation, moisture and precipitation relationships along the South Pacific Convergence Zone in reanalyses and CMIP5 models. *J. Clim.* **26**: 10174–10192.

Niznik MJ, Lintner BR, Matthews AJ, Widlansky MJ. 2015. The role of tropical-extratropical interaction and synoptic variability in maintaining the South Pacific Convergence Zone in CMIP5 models. *J. Clim.* **28**: 3353–3374, doi: 10.1175/JCLI-D-14 00527.1.

North GR, Bell TL, Cahalan RF. 1982. Sampling errors in the estimation of empirical orthogonal functions. *Mon. Weather Rev.* **110**: 699–706.

Qin J, Robinson WA. 1993. On the Rossby wave source and the steady linear response to tropical forcing. *J. Atmos. Sci.* **50**: 1819–1823.

Reynolds RW, Rayner NA, Smith TM, Stokes DC, Wang W. 2002. An improved in situ and satellite SST analysis for climate. *J. Clim.* **15**: 1609–1625.

Robertson AW, Mechoso CR. 2000. Interannual and interdecadal variability of the South Atlantic Convergence Zone. *Mon. Weather Rev.* **128**: 2947–2957.

Salinger MJ, McGree S, Beucher F, Power SB, Delage F. 2014. A new index for variations in the position of the South Pacific convergence zone 1910/11-2011/2012. *Clim. Dyn.* **43**: 881–892.

Slingo JM. 1987. The development and verification of a cloud prediction scheme for the ECMWF model. *Q. J. R. Meteorol. Soc.* **113**: 899–927.

Streten NA. 1973. Some characteristics of satellite-observed bands of persistent cloudiness over the Southern Hemisphere. *Mon. Weather Rev.* **101**: 486–495.

Takahashi K, Battisti DS. 2007a. Processes controlling the mean tropical Pacific precipitation pattern. Part I: The Andes and the eastern Pacific ITCZ. *J. Clim.* **20**: 3434–3451.

Takahashi K, Battisti DS. 2007b. Processes controlling the mean tropical Pacific precipitation pattern. Part II: The SPCZ and the southeast Pacific dry zone. *J. Clim.* **20**: 5696–5706.

Trenberth KE. 1976. Spatial and temporal variations of the Southern Oscillation. *Q. J. R. Meteorol. Soc.* **102**: 639–653.

Van der Wiel K, Matthews AJ, Stevens DP, Joshi MM. 2015a. A dynamical framework for the origin of the diagonal South Pacific and South Atlantic Convergence Zones. *Q. J. R. Meteorol. Soc.* **141**: 1997–2010, doi: 10.1002/qj.2508.

Van der Wiel K, Matthews AJ, Joshi MM, Stevens DP. 2015b. Why the South Pacific Convergence Zone is diagonal *Clim. Dyn.*. published online, doi: 10.1007/s00382-015-2668-0.

Vincent DG. 1994. The South Pacific Convergence Zone (SPCZ): A review. *Mon. Weather Rev.* **122**: 1949–1970.

Vincent EM, Lengaigne M, Menkes CE, Jourdain NC, Marchesiello P, Madec G. 2011. Interannual variability of the South Pacific Convergence Zone and implications for tropical cyclone genesis. *Clim. Dyn.* **36**: 1881–1896.

Widlansky MJ. 2010. 'Climate dynamics of the South Pacific Convergence Zone and similarities with other subtropical convergence zones in the southern hemisphere', PhD thesis. Georgia Institute of Technology: Atlanta, GA.

Widlansky MJ, Webster PJ, Hoyos CD. 2011. On the location and orientation of the South Pacific Convergence Zone. *Clim. Dyn.* **36**: 561–578.

Widlansky MJ, Timmermann A, Stein K, McGregor S, Schneider N, England MH, Lengaigne M, Cai W. 2013. Changes in South Pacific rainfall bands in a warming climate. *Nat. Clim. Change* **3**: 417–423.

Xie P, Arkin PA. 1997. Global precipitation: A 17-year monthly analysis based on gauge observations, satellite estimates, and numerical model outputs. *Bull. Am. Meteorol. Soci.* **78**: 2539–2558.

Zhong WY, Haigh JD. 1995. Improved broad-band emissivity parameterization for water vapor cooling calculations. *J. Atmos. Sci.* **52**: 124–138.

© 2015 Royal Meteorological Society